Inorganic Chemistry

ARTICLE

pubs.acs.org/IC

Introducing a Magnetic Guest to a Tetrel-Free Clathrate: Synthesis, Structure, and Properties of $Eu_xBa_{8-x}Cu_{16}P_{30}$ ($0 \leq x \leq 1.5$)

Kirill Kovnir,*[,†,‡] Ulrike Stockert,[†] Sergij Budnyk,[†,⊥] Yurii Prots,[†] Michael Baitinger,[†] Silke Paschen,[§] Andrei V. Shevelkov,[∥] and Yuri Grin[†]

[†]Max-Planck-Institut für Chemische Physik fester Stoffe, Nöthnitzer Straße 40, 01187 Dresden, Germany

[‡]Department of Chemistry, University of California, Davis, One Shields Avenue, Davis, California 95616, United States

[§]Institute of Solid State Physics, Vienna University of Technology, Wiedner Hauptstr. 8-10, 1040 Vienna, Austria

[∥]Chemistry Department, Lomonosov Moscow State University, Leninskie Gory 1-3, 119991, Moscow, Russia

Supporting Information

ABSTRACT: The europium-containing clathrate-I $Eu_xBa_{8-x}Cu_{16}P_{30}$ was synthesized from the elements. Powder X-ray diffraction in combination with energy dispersive X-ray absorption spectroscopy (EDXS) and metallographic studies showed the homogeneity range with $x \leq 1.5$. Determination of the crystal structure confirmed the presence of an orthorhombic superstructure of clathrate-I and revealed that Eu atoms exclusively resided in small pentagonal-dodecahedral cages. Magnetic measurements together with X-ray absorption spectroscopy are consistent with a $4f^7$ (Eu^{2+}) ground state for $Eu_xBa_{8-x}Cu_{16}P_{30}$. Below 3 K the Eu moments order antiferromagnetically. Resistivity measurements revealed metallic behavior of the investigated clathrate, in line with the composition deviating from the Zintl counting scheme. Local vibrations of the guest atoms inside the cages are analyzed with the help of specific heat investigations.

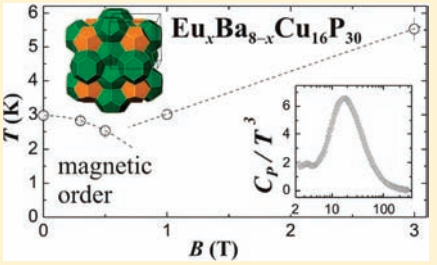

INTRODUCTION

Clathrates are inclusion or host−guest compounds containing a three-dimensional framework with large cavities, in which guest atoms are situated.[1] In classical neutral clathrates, hydrates of different gases and liquids, the framework is made up of water molecules and the guests are inert gas atoms or small inorganic (e.g., Cl_2, CO_2, H_2S) or organic molecules (viz. CH_4, C_3H_8, $(n\text{-}C_4H_9)_3SF$).[1] Intermetallic analogues of gas hydrates, binary silicides of alkali metals, were first reported in 1965.[2] The separate group of compounds was referred to as "intermetallic" (anionic) clathrates. For the past 40 years about 200 clathrates based on Si, Ge, and Sn were reported.[3] Over 30 compounds are known as cationic clathrates which contain P, S, As, Sb, Te, or I forming the frameworks, and Te, Cl, Br, or I as guest atoms. The term "tetrel" clathrates underlines that the framework of almost all clathrates is based on Si, Ge, and Sn. One of two known exceptions is $Ba_8Cu_{16}P_{30}$ with a framework composed of Cu and P atoms.[4,5] This compound is a unique representative of an orthorhombic superstructure of clathrate I with the symmetry of the space group *Pbcn*, $a = \sqrt{2}\,a_0$, $b = a_0$, $c = 2\sqrt{2}a_0$, where a_0 is the lattice parameter of the original cubic clathrate I structure.

The chemistry and physics of clathrates attract significant attention of the scientific community since they are regarded as perspective thermoelectric materials. According to the concept of "phonon glass-electron crystal",[6] cage compounds, in particular, clathrates, are expected to have low thermal (κ) but comparatively high electrical conductivity (σ). The combination of these properties gives rise to an enhancement of the dimensionless thermoelectric figure of merit $ZT = (S^2\sigma/\kappa)T$, with thermopower S and temperature T, which is a measure characterizing the thermal-to-electrical (or vice versa) energy conversion. Large thermopower values are crucial for achieving a high ZT value. The incorporation of rare-earth atoms as guests into the cages appears promising to further increase the thermoelectric figure-of-merit because possible hybridization of the localized 4f states of the rare-earth ions with the delocalized conduction electron states gives rise to an enhanced density of states at a Fermi level, leading to a larger thermopower. Up to now, only Eu-containing clathrates were synthesized,[7] and $Eu_8Ga_{16-x}Ge_{30+x}$ is the only one in which the guest positions are fully occupied by a rare-earth element.[8] Recently, some other clathrate I compounds with a general formula $Eu_xA_{8-x}[M_yE_{46-y}]$ (A = K, Sr, Ba; M = Al, Ga, Zn, Cd, Cu; E = Si, Ge) and a mixed occupancy of the cationic sites have been reported.[9] In all compounds Eu was found to be in the $4f^7$ (Eu^{2+}) state. Only one reported Eu-containing clathrate, namely, $Eu_2Ba_6Cu_4Ga_4Si_{38}$, contains a significant amount (8%) of transition metal atoms, Cu, in the framework. By contrast, $Ba_8Cu_{16}P_{30}$ exhibits the framework with 35% of copper atoms.[4] A comparably low thermal conductivity and a high thermoelectric power leading to a dimensionless figure of merit ZT = 0.02 at 300 K were reported for $Ba_8Cu_{16}P_{30}$.[5] For crystal chemical considerations, $Ba_8Cu_{16}P_{30}$ appears to be a promising starting material for a Ba−Eu exchange with the aim

Received: July 12, 2011
Published: September 12, 2011

of improving the thermoelectric properties, especially at low temperatures. Furthermore, its unique chemical and crystallographic position among the large group of clathrate I compounds calls for a fundamental and detailed study of the effect of cationic substitution inside the cages. In the present work we report on the influence of the Eu-substitution on the structural and physical properties of the clathrate I derivative $Eu_xBa_{8-x}Cu_{16}P_{30}$ ($0 \leq x \leq 1.5$).

EXPERIMENTAL SECTION

Synthesis. Samples with nominal compositions $Eu_xBa_{8-x}Cu_{16}P_{30}$ (x = 0 to 3 with a step of 0.5) were prepared by a solid-state reaction. All manipulations with the samples and initial materials were performed inside an argon-filled glovebox ($p(O_2)$, $p(H_2O) \leq 1$ ppm). The starting materials, barium (Alfa Aesar, 99.9%), distilled europium (starting material, Lamprecht, 99.9%), copper powder (Chempur, 99.99%), and red phosphorus (Chempur 99.999%), were mixed in appropriate amounts and pressed into pellets, which were placed into glassy-carbon crucibles, and subsequently sealed inside quartz ampules in Ar atmosphere (~300 mbar). The ampules were heated to 1125 K in 24 h, kept for 120 h, and cooled to room temperature. The resulting products were reground, pressed, and annealed for 240 h at 1125 K under the same conditions. The samples for measuring the physical properties of $Eu_xBa_{8-x}Cu_{16}P_{30}$ were prepared by a similar technique but utilizing a higher temperature (1135 K) and a longer duration of the second annealing (one month), see the Results and Discussion section for explanation. Additionally, the synthesis of the sample $Ba_8Cu_{16}P_{30}$ was performed according to the procedure described in the literature.[4] Also, a procedure for the preparation of high-quality single crystals using CuCl as a flux was utilized for $Eu_xBa_{8-x}Cu_{16}P_{30}$ samples.[4] Hereby, Eu, Ba, CuCl, and P were mixed in an 8:8:16:30 molar ratio and annealed at 1125 K for 120 h. Formed Ba and Eu chlorides were washed away with water.

The annealed samples contained numerous silvery plate-like crystals stable in air for at least several months and resistant to the treatment by diluted hydrochloric acid (1:1). Powdered samples have a gray color and are stable in air within at least a few weeks.

Metallography and EDXS. Samples for metallographic investigations were prepared by grinding and polishing the prepared ingots under inert conditions in an argon-filled glovebox. Homogeneity of the microstructures and phase distribution were examined by optical microscopy (Zeiss Axioplan2) in bright-field and polarized light. The semiquantitative analysis was performed by energy dispersive X-ray absorption spectroscopy (EDXS) on the metallographic section (Philips SX-30 scanning electron microscope, standard-less method). Precise determination of the Ba:Eu ratio was hampered by the overlapping of their EDX spectra.

X-ray Powder Diffraction. The samples were characterized by X-ray powder diffraction (XRD) using a Huber Image Plate Camera G670. For routine experiments CuKα_1 radiation with λ = 1.540598 Å was used, while for the precise determination of the unit cell parameters CrKα_1 radiation with λ = 2.2897 Å was employed to get a better resolution of the reflections. The unit cell parameters of $Eu_xBa_{8-x}Cu_{16}P_{30}$ were refined from the same set of 90 Bragg reflections for each sample (all with intensity >2%) using LaB_6 (cubic, a = 4.15692 Å) as an internal standard and the WinCSD program package for the calculations.[10]

Crystal Structure Determination. Several plate-shaped crystals of $Eu_xBa_{8-x}Cu_{16}P_{30}$ were picked up from the samples with x = 1.5 and 2.0 after the second annealing or from products of the CuCl flux-assisted synthesis. Three data sets were collected from the qualitatively best single crystals obtained from three different batches (from both flux and standard synthesis) on a Rigaku AFC7 diffractometer (graphite monochromator, MoKα radiation, Mercury CCD detector). All three crystals had lattice parameters equal within 3 estimated standard deviations and showed similar residual values and chemical composition with x = 1.5. Thus, the structural data for one crystal are presented and discussed hereafter. Numerical absorption correction was performed by a multiscan routine. Details of the X-ray diffraction experiment are presented in Table 1. The crystal structure was solved by direct methods. The refinement of the crystal structure was performed with the WinCSD program package.[10] The atomic coordinates and selected interatomic distances are listed in Tables 2–4. The atomic coordinates were standardized by the STRUCTURE TIDY program.[11]

Table 1. Data Collection and Structure Refinement Parameters for $Eu_{1.5}Ba_{6.5}Cu_{16}P_{30}$[a]

composition	$Eu_{1.51(3)}Ba_{6.49}Cu_{16}P_{30}$
space group	*Pbcn* (no. 60)
temperature [K]	293(2)
a [Å]	14.0669(5)
b [Å]	10.0625(4)
c [Å]	27.967(1)
V [Å^3]	3958.7(5)
Z	4
λ [Å]	MoK_α, 0.71073
density [g cm^{-3}]	5.157
μ [mm^{-1}]	18.295
2θ range [deg.]	$2.5 < \theta < 31.9$
reflection measured	30454
independent reflections	6120 [R_{int} = 0.045]
reflections used for refinement	3654
parameters refined	251
R_1, $F_o > 4\sigma F_o$	0.033
R_1, all data	0.072
largest diff. peak and hole [e/Å^3]	2.40 and −1.78

[a] Further details of the crystal structure determination may be obtained from Fachinformationszentrum Karlsruhe, D-76344 Eggenstein-Leopoldshafen, Germany, on quoting the depository number CSD-423229.

Thermal Behavior. Differential scanning calorimetry (DSC) investigations of the $Eu_xBa_{8-x}Cu_{16}P_{30}$ samples were performed with the Netzsch STA 409 EP equipment in a quartz glass crucibles sealed under vacuum in the temperature range from 300 to 1270 K with a heating rate of 5 K/min.

X-ray Absorption Spectroscopy (XAS). The Eu L_{III} X-ray absorption spectra of polycrystalline $Eu_xBa_{8-x}Cu_{16}P_{30}$ samples were recorded in a transmission mode at the EXAFS II beamline E4 of HASYLAB at DESY. Wavelength selection was realized by means of a Si(111) double crystal monochromator, which corresponds to an experimental resolution of approximately 2 eV (fwhm) at the Eu L_{III} threshold of 6977 eV. Eu_2O_3 was used as an external reference for energy calibration.

Physical Properties. Investigations of the direct current (dc) magnetic susceptibility and magnetization were performed in 1.8–300 K temperature range using a SQUID magnetometer (Quantum Design MPMS). Specific heat and resistivity were studied with a commercial multipurpose measurement device (Quantum Design PPMS) in fields up to 3 T. Investigations of the electrical resistivity have been carried out between 0.35 and 300 K with a standard 4-point alternating current (ac) technique at 31 Hz. The specific heat was measured with a relaxation time method in the temperature range from 2 to 300 K.

RESULTS AND DISCUSSION

Synthesis, Thermal and Compositional Stability. In a first step, the synthesis of $Ba_8Cu_{16}P_{30}$ was reproduced according to the literature.[4] It was reported that the synthesis from stoichiometric

Table 2. Atomic Coordinates and Equivalent Displacement Parameters for $Eu_{1.51(3)}Ba_{6.49}Cu_{16}P_{30}$

atom	site	*x*/*a*	*y*/*b*	*z*/*c*	B_{eq}
Eu(1)	4*c*	0	−0.00883(7)	1/4	0.87(1)
$Eu_{0.51(3)}Ba_{0.49}(2)$	4*b*	0	1/2	0	0.83(1)
Ba(1)	8*d*	0.25027(6)	0.24563(6)	0.37622(2)	1.22(1)
Ba(2)	8*d*	0.87450(5)	−0.00829(6)	0.44098(2)	1.16(1)
Ba(3)	8*d*	0.37847(5)	0.00644(7)	0.18485(2)	1.32(1)
Cu(1)	8*d*	0.31382(9)	0.3140(1)	0.25042(5)	0.94(3)
Cu(2)	8*d*	0.5010(1)	0.1803(1)	0.40737(4)	0.82(3)
Cu(3)	8*d*	0.62276(9)	0.0002(1)	0.18963(4)	0.88(2)
Cu(4)	8*d*	0.05597(9)	0.1882(1)	0.46814(5)	0.98(3)
Cu(5)	8*d*	0.09256(8)	−0.0041(1)	0.35644(4)	0.97(2)
Cu(6)	8*d*	0.28408(8)	−0.0052(1)	0.45429(4)	0.92(2)
Cu(7)	8*d*	0.15149(9)	0.1165(1)	0.17273(5)	1.02(3)
Cu(8)	8*d*	0.3435(1)	0.1197(1)	0.57755(5)	0.96(3)
P(1)	8*d*	−0.0038(2)	0.1861(2)	0.15818(8)	0.68(5)
P(2)	8*d*	0.4955(2)	0.3129(2)	0.15848(8)	0.60(5)
P(3)	8*d*	0.6852(2)	0.1912(3)	0.49901(8)	0.62(5)
P(4)	8*d*	0.3130(2)	0.1877(3)	0.49951(8)	0.62(5)
P(5)	8*d*	0.0005(2)	0.3221(2)	0.40438(9)	0.67(5)
P(6)	8*d*	0.7484(2)	0.2442(3)	0.37526(8)	0.57(4)
P(7)	8*d*	0.4366(2)	0.3064(3)	0.47027(9)	0.71(5)
P(8)	8*d*	0.4043(2)	−0.0053(3)	0.39309(8)	0.66(4)
P(9)	8*d*	0.7884(2)	0.0011(3)	0.20256(8)	0.68(4)
P(10)	8*d*	0.1845(2)	0.1756(2)	0.25179(9)	0.62(5)
P(11)	8*d*	0.1225(2)	−0.0093(2)	0.43858(7)	0.52(4)
P(12)	8*d*	0.1515(2)	0.1250(2)	0.67218(8)	0.57(5)
P(13)	8*d*	0.5546(2)	0.1939(3)	0.22168(9)	0.77(5)
P(14)	8*d*	0.6587(2)	0.1210(2)	0.42311(9)	0.58(5)
P(15)	8*d*	0.9380(2)	0.2978(3)	0.21895(9)	0.65(5)

amounts of elements was unsuccessful and resulted in exclusive formation of another ternary phase, $BaCu_2P_4$,[12] having a composition close to the clathrate phase ($Ba_8Cu_{16}P_{30} = BaCu_2P_{3.75}$). Therefore, for the synthesis of $Ba_8Cu_{16}P_{30}$, the elements (Ba, Cu, and P) were taken in a ratio of 1:1:3. A two-step synthesis (annealing at 1073 K, cooling down to room temperature, regrinding, annealing at 1103 K) resulted in a sample containing $Ba_8Cu_{16}P_{30}$ and admixtures of barium phosphides (mainly BaP_3). The phosphide admixtures were removed by washing with a mixture of acetic acid and hydrogen peroxide (30%). Thus, the synthesis described by Dünner and Mewis was reproduced.[4] Careful powder X-ray diffraction examination of the products after washing indeed revealed only the diffraction peaks belonging to the clathrate phase. However, a very broad additional peak (halo) at a $2\theta \approx 30°$ was found, which may indicate the presence of an amorphous phase. To check this possibility, the washed sample was carefully dried and annealed in evacuated and sealed quartz ampules at 1103 K for 5 days. The following X-ray diffraction analysis clearly showed the presence of the barium hydrogen phosphate $BaHPO_4$ in the sample. Apparently, during oxidizing washing of the barium phosphides, the amorphous barium *phosphates* were produced. This makes the described synthetic technique inappropriate for synthesis of Eu-containing phases, since Eu phosphates might contribute to magnetic properties of the sample.

To optimize the synthetic procedure, the thermal behavior of the $Ba_8Cu_{16}P_{30}$ sample was checked. Differential scanning calorimetry (DSC) reveals that $Ba_8Cu_{16}P_{30}$ is stable below 1134(5) K (Figure 1). Indeed, only one peak corresponding to the decomposition of the clathrate phase was observed during heating at 1134 K. A sample of $Ba_8Cu_{16}P_{30}$ was then successfully synthesized from stoichiometric amounts of the elements at 1125 K as described in Experimental Section. According to XRD as well as metallographic and SEM investigations the sample consists of a single-phase clathrate I with the $Ba_8Cu_{16}P_{30}$ composition. Specifically, no admixture of $BaCu_2P_4$ was observed.

The samples with the nominal composition $Eu_xBa_{8-x}Cu_{16}P_{30}$ were synthesized in a similar way. The DSC investigations of the $Eu_xBa_{8-x}Cu_{16}P_{30}$ compounds show that they are stable in almost

Table 3. Selected Interatomic Distances (Å) in the Framework of $Eu_{1.51(3)}Ba_{6.49}Cu_{16}P_{30}$

atoms	distance	atoms	distance	atoms	distance
Cu(1)−P(10)	2.291(3)	Cu(5)−P(1)	2.322(3)	P(1)−P(15)	2.195(3)
Cu(1)−P(12)	2.324(3)	Cu(5)−P(2)	2.329(3)	P(1)−P(5)	2.222(3)
Cu(1)−P(9)	2.324(3)	Cu(5)−P(11)	2.336(3)	P(2)−P(12)	2.194(4)
Cu(1)−P(13)	2.344(3)	Cu(5)−P(9)	2.359(3)	P(2)−P(13)	2.291(3)
Cu(2)−P(2)	2.275(3)	Cu(6)−P(11)	2.316(3)	P(3)−P(4)	2.172(4)
Cu(2)−P(14)	2.339(3)	Cu(6)−P(3)	2.323(3)	P(3)−P(14)	2.268(3)
Cu(2)−P(8)	2.345(3)	Cu(6)−P(4)	2.352(3)	P(4)−P(7)	2.263(4)
Cu(2)−P(7)	2.350(3)	Cu(6)−P(8)	2.407(3)	P(5)−P(8)	2.215(3)
Cu(3)−P(8)	2.346(2)	Cu(7)−P(6)	2.331(3)	P(6)−P(14)	2.218(3)
Cu(3)−P(13)	2.350(3)	Cu(7)−P(1)	2.331(3)	P(6)−P(12)	2.313(3)
Cu(3)−P(15)	2.357(3)	Cu(7)−P(10)	2.337(3)	P(7)−P(11)	2.218(3)
Cu(3)−P(11)	2.359(3)	Cu(7)−P(12)	2.431(3)	P(9)−P(10)	2.203(3)
Cu(4)−P(11)	2.348(3)	Cu(8)−P(6)	2.324(3)	P(10)−P(15)	2.270(4)
Cu(4)−P(5)	2.367(3)	Cu(8)−P(4)	2.327(3)	P(13)−P(13)	2.207(4)
Cu(4)−P(3)	2.370(3)	Cu(8)−P(5)	2.341(3)	P(15)−P(15)	2.461(4)
Cu(4)−P(7)	2.405(3)	Cu(8)−P(14)	2.423(3)		

Table 4. Shortest Guest-Framework Distances (Å) for $Eu_{1.51(3)}Ba_{6.49}Cu_{16}P_{30}$

atoms	distance	atoms	distance
Eu(1)−P(2)	3.125(2)	Ba(2)−Cu(4)	3.270(1)
Eu(1)−Cu(1)	3.168(1)	Ba(2)−Cu(8)	3.306(2)
Eu(1)−P(13)	3.188(3)	Ba(2)−Cu(4)	3.317(1)
Eu(1)−P(10)	3.192(2)	Ba(2)−P(7)	3.324(3)
Eu(1)−P(1)	3.232(2)	Ba(2)−P(14)	3.341(3)
Eu(1)−Cu(5)	3.250(1)	Ba(2)−P(7)	3.347(3)
		Ba(2)−P(11)	3.373(3)
Eu/Ba(2)−Cu(2)	3.163(1)	Ba(2)−P(12)	3.396(2)
Eu/Ba(2)−P(5)	3.218(2)		
Eu/Ba(2)−P(4)	3.238(3)	Ba(3)−P(14)	3.275(3)
Eu/Ba(2)−P(3)	3.240(3)	Ba(3)−P(13)	3.281(3)
		Ba(3)−Cu(8)	3.295(3)
Ba(1)−P(9)	3.347(2)	Ba(3)−P(13)	3.358(3)
Ba(1)−P(8)	3.351(3)	Ba(3)−Cu(7)	3.396(2)
Ba(1)−Cu(6)	3.260(1)		
Ba(1)−P(8)	3.361(3)		
Ba(1)−Cu(6)	3.371(1)		
Ba(1)−Cu(5)	3.396(1)		
Ba(1)−Cu(5)	3.398(1)		

dx.doi.org/10.1021/ic201474h |*Inorg. Chem.* 2011, 50, 10387–10396

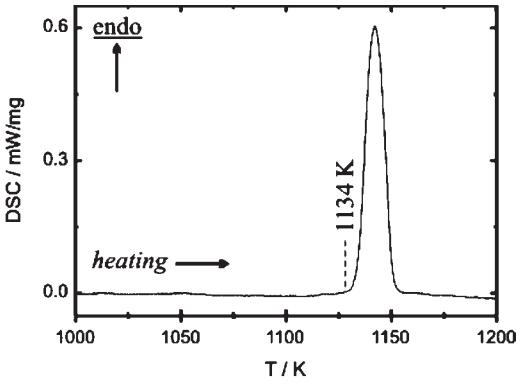

Figure 1. Thermal behavior of $Ba_8Cu_{16}P_{30}$ in vacuum.

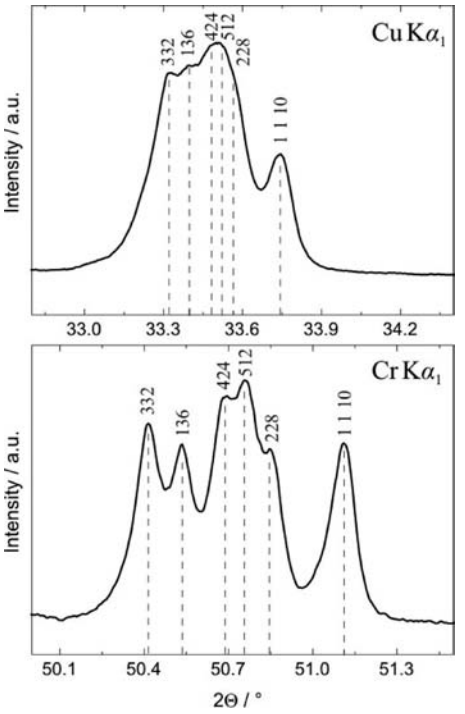

Figure 2. Fragment of the powder XRD pattern of $Eu_xBa_{8-x}Cu_{16}P_{30}$ collected with CuKα_1 (top) and CrKα_1 (bottom) radiation. Calculated Bragg peaks positions are indicated with dotted lines.

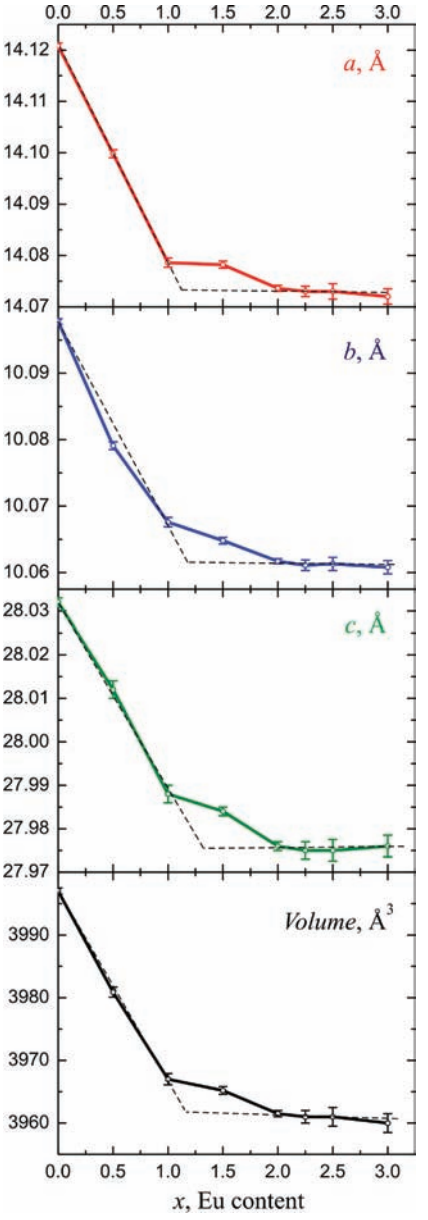

Figure 3. Dependence of the unit cell parameters and volume of $Eu_xBa_{8-x}Cu_{16}P_{30}$ on the nominal Eu content, x. Dashed black lines are drawn to guide the eyes to indicate the limits of the unit cell.

the same temperature range as $Ba_8Cu_{16}P_{30}$. XRD reveals that the samples with nominal $x = 0$, 0.5, and 1.0 were phase pure, while the sample with $x = 1.5$ contained small amounts ($\sim$ 2%) of Ba_3P_2. The samples with a nominal Eu content $x \geq 2$ contained significant amounts ($\sim$ 10%) of $EuCu_{1.75}P_2$.[13] A precise determination of the unit cell parameters was possible only upon utilizing Cr Kα_1 radiation, since the $Eu_xBa_{8-x}Cu_{16}P_{30}$ reflections were not well resolved when CuKα_1 radiation was used (Figure 2). The unit cell volume is decreasing upon the substitution of Eu for Ba (Figure 3), which is reasonable since $r(Eu^{2+}) < r(Ba^{2+})$.[14] Despite of orthorhombic symmetry, the crystal structure collapses isotropically with increasing Eu content, all the unit cell parameters change in similar way (Figure 3). From XRD data one can conclude that the Eu content does not exceed $x = 1.5$.

The results of the metallographic and EDXS analyses agree with the XRD ones. Samples with $x = 0.5$ and 1.0 are nearly phase pure with just minor (<1%) admixtures of the $EuCu_{1.75}P_2$ phase. The amount of such admixture increases with increasing x, reaching considerable ($\sim$ 10%) values at $x = 2$. Overlapping of Eu and Ba EDX spectra resulted in relatively high uncertainties in the Eu and Ba concentrations. Nevertheless, the Eu/Ba ratio (Table 5) determined by EDXS deviates substantially from the starting composition for the high x values thus confirming the compositional limit of the investigated solid solution concluded from XRD. Synthesis performed at higher temperature (1135 K) results in maximum Eu content of $x = 1.5$, thus fully confirming results of powder and single crystal X-ray diffraction experiments.

The $Eu_xBa_{8-x}Cu_{16}P_{30}$ samples with $x \geq 1$ contain admixtures of Eu-containing ternary phases, which hamper the detailed investigation of the physical properties of the Eu-containing clathrate phase. Application of a higher synthesis temperature

dx.doi.org/10.1021/ic201474h |Inorg. Chem. 2011, 50, 10387–10396

Table 5. Results of the EDX Analysis of the $Eu_xBa_{8-x}Cu_{16}P_{30}$ Samples Synthesized at 1125 and 1135 K

	x, europium content	
nominal	1125 K	1135 K
0.5	0.6(2)	
1.0	0.9(2)	1.0(2)
1.5	1.0(2)	1.5(2)
2.0	1.3(2)	1.6(2)

(1135 K) leads to partial melting of the clathrate phase while the admixture phases remain solid. After one month of annealing, the admixtures tend to segregate to the outer part of the ingot leaving the single-phase clathrate in the inner part. This was confirmed by metallographic and EDXS investigations as well as by XRD. The single-phase inner parts of the ingots were cut with a wire saw and used for investigations of the physical properties.

All our attempts to synthesize $R_xBa_{8-x}Cu_{16}P_{30}$ (R = Ce, Sm, Yb) resulted in the formation of the clathrate I phase together with admixtures of *R*-Cu-P ternary phases. The unit cell parameters for the formed clathrate phase were the same as for $Ba_8Cu_{16}P_{30}$ within one estimated standard deviation. EDXS shows that the produced clathrate phases did not contain a rare-earth metal.

Crystal Structure of $Eu_xBa_{8-x}Cu_{16}P_{30}$. Several single crystals selected from the products of the syntheses of $Eu_xBa_{8-x}Cu_{16}P_{30}$ with x = 1.5 and 2 as well as single crystals produced by the flux method were tested. All of them clearly exhibit a formation of the orthorhombic superstructure of clathrate I. The structure solution for the single crystal selected from flux synthesis was performed by direct methods which allow location of all atomic positions in the unit cell. All guest atoms were set as Ba. The subsequent refinement showed that atomic displacement parameters (ADPs) for the Ba(1) and Ba(2) positions were notably smaller than those of the other three Ba atoms (~0.4 vs ~1.2). In a second step, those two positions were refined as mixed occupied by Ba and Eu. It turned out that both elements occupy the Ba(2) position in an equimolar ratio, while the other position is occupied almost exclusively by Eu. Furthermore, the refinement of the framework positions occupancies confirmed the $Cu_{16}P_{30}$ composition and absence of mixed Cu/P occupancies. Refinement of the mixed Eu/Ba occupancy for three positions inside large tetrakaidecahedra reveals that these positions are solely occupied by Ba. The final refinement in the *Pbcn* space group with anisotropic atomic displacement parameters for all atoms converged to R_1 = 0.033. Investigations of other two single crystals revealed very similar Eu content and distribution over the guest positions and the likewise vacancy/disorder-free clathrate framework $Cu_{16}P_{30}$.

$Eu_xBa_{8-x}Cu_{16}P_{30}$ is isostructural to the parent phase $Ba_8Cu_{16}P_{30}$[4] and exhibits the same type of the clathrate I superstructure, space group *Pbcn* (no. 60), $a = \sqrt{2}a_0$, $b = a_0$, $c = 2\sqrt{2}a_0$ (Figure 4), where a_0 is the lattice parameter of the clathrate I structure motif. The type-I clathrate structure contains two types of polyhedral cages (Figure 4 top), the 20-vertex pentagonal dodecahedra $[5^{12}]$ and larger 24-vertex 14-face tetrakaidecahedra $[5^{12}6^2]$ (see ref 15 for polyhedra notation). The formula of the ideal clathrate I is G_8E_{46} with G a guest and E a framework atom. Several variants of clathrate I superstructures with volume increase are reported: $Sn_{14}In_{10}P_{21.2}\square_{0.8}I_8$ (tetragonal, $P4_2/m$, $V = 5V_0$), $Ba_8Ge_{43}\square_3$ and $Rb_8Sn_{44}\square_2$ (cubic, $Ia\bar{3}d$, $V = 8V_0$),

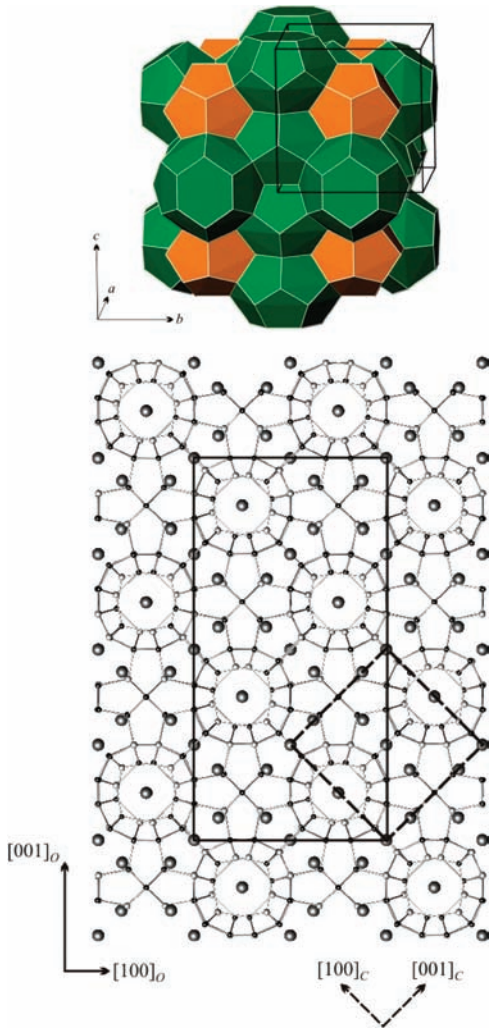

Figure 4. Top: polyhedral representation of the crystal structures of clathrate I; pentagonal dodecahedra, orange; tetrakaidecahedra, green. Bottom: crystal structure of $Eu_xBa_{8-x}Cu_{16}P_{30}$. Bold solid lines show the unit cell; bold dashed lines show the unit cell of a prototype cubic clathrate I structure. Ba/Eu: large gray; Cu: small white; P: small black.

$Sn_{20.5}\square_{3.5}As_{22}I_8$ (cubic, $F23$, $V = 8V_0$).[16] In all cases the superstructure formation is accompanied by partial or full ordering of the vacancies in the clathrate framework. By contrast, the compound $Ba_8Cu_{16}P_{30}$ is vacancy-free, thus having the ideal clathrate I composition with 8 guest and 46 framework atoms per formula unit and with the copper atoms always coordinated by four phosphorus atoms.

In the ideal structure of clathrate I (space group $Pm\bar{3}n$, no. 223) Cu and P atoms are expected to be distributed over three atomic positions −6*c*, 16*i*, and 24*k*. An atom in the position 6*c* is surrounded only by atoms in the position 24*k*, while atoms in the positions 24*k* and 16*i* always form homonuclear bonds with the neighboring atoms in the same position. Taking into account that copper atoms should always have an environment of four phosphorus atoms and no copper−copper bonds are expected, the only possible way to build a cubic unit cell of the clathrate I framework from 16 Cu and 30 P atoms would be to allow mixed occupancy of all positions by Cu and P. Instead of such mixing, copper and phosphorus atoms order in the crystal structure of $Eu_xBa_{8-x}Cu_{16}P_{30}$, yielding a larger unit cell with orthorhombic

dx.doi.org/10.1021/ic201474h |*Inorg. Chem.* 2011, 50, 10387–10396

Scheme 1. Group−Subgroup Relationship for $Ba_8Cu_{16}P_{30}$ and Splitting of the Wyckoff Positions during the Transformation from the Ideal Clathrate-I Space Group $Pm\bar{3}n$ to the *Pbcn* Space Group

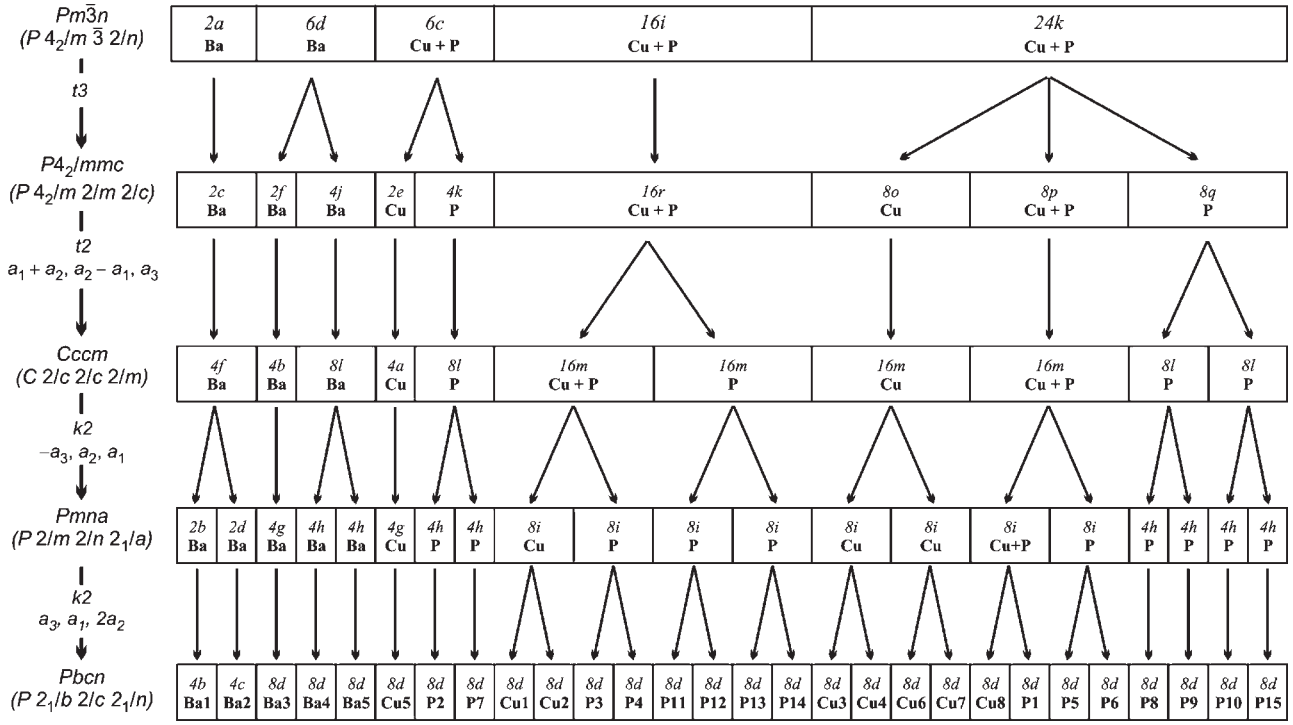

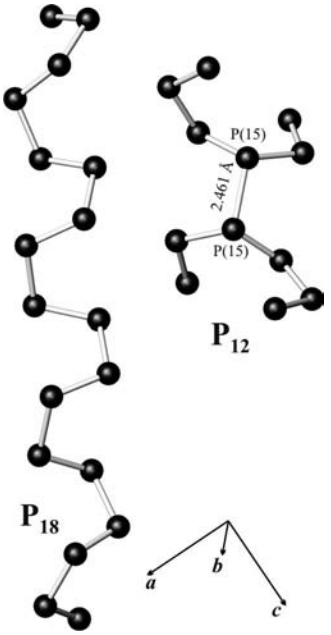

Figure 5. Finite homonuclear fragments P_{18} and P_{12} present in the crystal structure of $Eu_xBa_{8-x}Cu_{16}P_{30}$ in a 1:1 ratio.

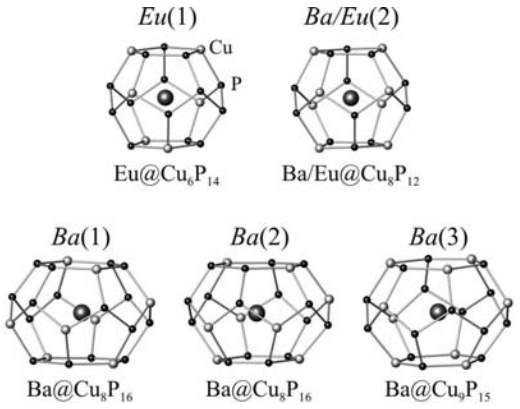

Figure 6. Coordination of the guest atoms in $Eu_xBa_{8-x}Cu_{16}P_{30}$. Eu/Ba: large gray; Cu: small white; P: small black.

symmetry. It should be noted that the group *Pbcn* is not the maximal nonisomorphic subgroup of the space group $Pm\bar{3}n$ according to International Tables for Crystallography.[17] This group-subgroup relation can be described as a combination of "*klassengleich*" (class-equivalent) and "*translationengleich*" (lattice-equivalent) symmetry reductions.[18] The corresponding symmetry relations are shown in Scheme 1. It is apparent that the mixed occupancy of the cubic 6*c* position is eliminated already in the group $P4_2/mmc$. A further decrease of the symmetry down to the space group *Pmna* is necessary to remove mixed occupancy from the cubic position 16*i*. However, in the *Pmna* space group one of the 8*i* positions originating from the cubic 24*k* position would still have a mixed occupation of Cu and P. Only in the case of the superstructure space group *Pbcn* there is no mixed occupancy of any framework position by atoms of different chemical nature. Clathrates $Sn_{19.3}Cu_{4.7}Pn_{22}I_8$ containing Cu and pnicogen (Pn = P, As) in the framework were reported; in these clathrates Cu and Pn occupied different framework positions.[19] Analysis of the ICSD database indicates that there are no structurally characterized metal phosphides with joint occupancy of one crystallographic position

dx.doi.org/10.1021/ic201474h |*Inorg. Chem.* 2011, 50, 10387–10396

by Cu and P.[20] Probably the different chemical nature of copper and phosphorus is a driving force for formation of unique orthorhombic superstructure of $Eu_xBa_{8-x}Cu_{16}P_{30}$.

Another example of changing the symmetry of clathrate I to avoid mixed framework occupancies was first reported by von Schnering et al. for the compounds with the general formula $G_8[Ge_{38}Pn_8]$ (G = Cl, Br, I; Pn = P, As, Sb).[21] These compounds crystallize in the noncentrosymmetric derivative of the space group $Pm\bar{3}n$, namely, $P4\bar{3}n$. The loss of the inversion center leads to a splitting of only one Wyckoff position, 16*i*, onto two 8-fold positions, one of them occupied by Ge and the other one by pnicogen Pn. In this case the symmetry reduction is not accompanied by metric changes of the unit cell.

In the crystal structure of the $Eu_xBa_{8-x}Cu_{16}P_{30}$ clathrate, the Cu−P distances (Table 3) are similar to those in the parent phase $Ba_8Cu_{16}P_{30}$ and the other ternary phosphides, such as $BaCu_2P_4$, or $EuCu_{1.75}P_2$.[12,13] While Cu is tetrahedrally coordinated by four P atoms, the latter ones have different coordination varying from 3Cu+1P to 1Cu+3P. Phosphorus atoms in $Eu_xBa_{8-x}Cu_{16}P_{30}$ form two finite homoatomic fragments, P_{12} and P_{18}, present in the crystal structure in a 1:1 ratio (Figure 5). P_{18} is a finite example of a helical chain $_\infty^1(P^-)$ often present in polyphosphides,[22] while P_{12} has a scorpion-like shape. To the best of our knowledge both phosphorus fragments are unique. Most of the P−P distances lying in the range of 2.17−2.32 Å are compatible with the single P−P bond.[22] However, the distance P(15)−P(15) is significantly longer, 2.461 Å (Figure 5). Nonetheless, the refinement of the occupancy of P(15) clearly shows that this position is exclusively occupied by phosphorus. In ordered polyphosphides a comparably large d(P−P) = 2.37 Å was previously reported only for a high-pressure phase of BaP_8.[23]

In the framework of $Eu_xBa_{8-x}Cu_{16}P_{30}$ five crystallographically independent cages are formed: two pentagonal dodecahedra and three tetrakaidecahedra (Figure 6). Eu atoms occupy the smaller cages, which is typical for Eu/Ba substituted clathrates[9] and may be understood from the smaller radius of Eu. However, the distribution of the Eu atoms is not statistical: Eu fully occupies the Cu_6P_{14} cage and only partially the Cu_8P_{12} cage. The shortest Eu−Cu distances are similar for both cages, 3.16−3.17 Å, while the Eu(1)−P(2) distance in the Cu_6P_{14} cage is significantly shorter than the Eu(2)−P(5) separation in the Cu_8P_{12} cage, 3.12 Å vs 3.22 Å (Table 4). Thus, the smaller Eu prefers to reside in the cages with the shortest guest-framework interaction. A similar preferred occupation of two different pentagonal-dodecahedral voids was observed for the $Si_{46-x}P_xTe_y$ clathrate I, where the tellurium vacancy formed in the cage having the shortest (∼ 3.1 Å) guest-framework distances.[24]

According to the Zintl concept the four-bonded clathrate I framework $[E_{46}]$ requires four electrons per atom for the formation of 2*c*-2*e* bonds, that is, 46 × 4 = 184 e^- per formula unit.[3,25] Such a charge-balanced compound is expected to exhibit semiconducting behavior because of the lack of free charge carriers. In the case of $Ba_8Cu_{16}P_{30}$, copper and phosphorus are expected to provide one and five valence electrons, respectively. Assuming that Ba transfers two valence electrons to the framework being Ba^{2+}, the total number of electrons per formula unit is 8 × 2 + 16 × 1 + 30 × 5 = 182 e^-. Thus, two electrons are missing compared to the Zintl counting scheme. The resulting charge carriers (holes) are held responsible for the reported metallic properties of $Ba_8Cu_{16}P_{30}$.[5] Opposite to barium, europium can be divalent or trivalent. Therefore, partial substitution of Eu for Ba may affect the number of charge carriers in

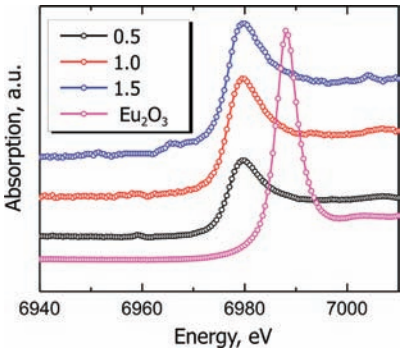

Figure 7. Room temperature Eu L_{III} X-ray absorption spectra of $Eu_xBa_{8-x}Cu_{16}P_{30}$ for different x in comparison with Eu_2O_3.

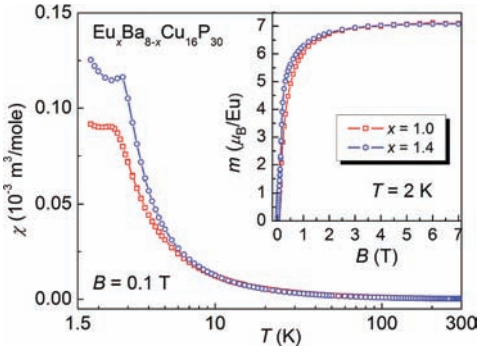

Figure 8. Magnetic properties of $Eu_xBa_{8-x}Cu_{16}P_{30}$ (x = 1 and 1.4). The main plot shows the temperature dependence of the magnetic susceptibility, $\chi(T)$, per mole Eu in an external magnetic field of B = 0.1 T. The inset displays the field dependence of the magnetic moment per Eu at 2 K.

$Eu_xBa_{8-x}Cu_{16}P_{30}$. Particularly, $Eu_2Ba_6Cu_{16}P_{30}$ is expected to be a semiconductor in the case of the Eu^{3+} $^7F_0$ ground state. Therefore XAS investigations were performed to determine the Eu oxidation state in $Eu_xBa_{8-x}Cu_{16}P_{30}$.

X-ray Absorption Spectroscopy (XAS). The Eu L_{III} X-ray absorption spectra of $Eu_xBa_{8-x}Cu_{16}P_{30}$ samples are dominated by the main signal at 6980 eV (Figure 7). This value is characteristic of the $4f^7$ $^8S_{7/2}$ (Eu^{2+}) ground state and approximately 9 eV smaller than the one observed for the Eu^{3+} $^7F_0$ ground state in the reference Eu_2O_3. The presence of divalent Eu is in accordance with the magnetic properties (vide infra). Mixed-valent Eu compounds (e.g., $Eu_{0.2}Pr_{0.8}Co_2P_2$) typically exhibit two distinct XAS peaks separated by ∼10 eV,[26] which is not the case for $Eu_xBa_{8-x}Cu_{16}P_{30}$. Thus, the Ba/Eu substitution appears to be isovalent and $Eu_xBa_{8-x}Cu_{16}P_{30}$ is expected to retain metallic properties of the $Ba_8Cu_{16}P_{30}$ compound.

Physical Properties of $Eu_xBa_{8-x}Cu_{16}P_{30}$ (x = 0, 1.0, and 1.4). Investigations of the physical properties were performed on the samples synthesized at 1135 K for two compositions of $Eu_xBa_{8-x}Cu_{16}P_{30}$ with a nominal Eu concentration x = 1.0 and 1.5. As a reference compound for the specific heat, the Eu-free $Ba_8Cu_{16}P_{30}$ was reinvestigated. Characterization with metallographic and EDXS analyses confirmed the single-phase nature of the investigated samples. The effective Eu content determined by EDXS was close to the nominal. Detailed examination of the physical properties indicates that actual Eu content in the second

dx.doi.org/10.1021/ic201474h |*Inorg. Chem.* 2011, 50, 10387–10396

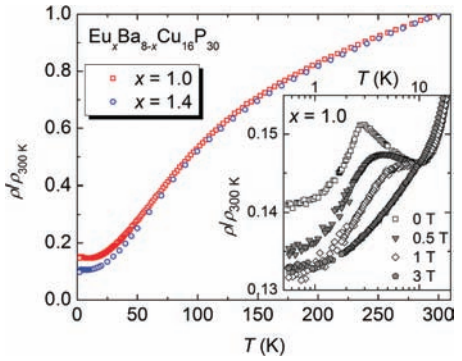

Figure 9. Temperature dependence of the electrical resistivity of $Eu_xBa_{8-x}Cu_{16}P_{30}$ (x = 1 and 1.4). The inset shows the low-temperature behavior of the sample with x = 1 in different magnetic fields.

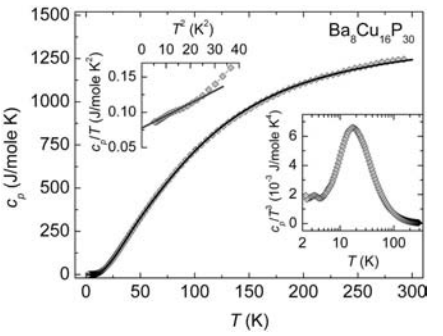

Figure 10. Temperature dependence of the specific heat c_p of $Ba_8Cu_{16}P_{30}$. In the main plot the data are shown with squares, whereas the line is a fit as described in the text. The upper left inset displays the low-T part as c_p/T vs T^2. The electronic contribution is estimated from the linear fit. In the lower right inset the data are plotted as c_p/T^3 vs T. The large maximum at around 18 K is indicative of an Einstein contribution.

sample is lower, namely, x = 1.4.[27] This Eu content is used hereafter.

At low temperatures the magnetic susceptibility of all samples strongly increases (Figure 8). $Eu_1Ba_7Cu_{16}P_{30}$ and $Eu_{1.4}Ba_{6.6}Cu_{16}P_{30}$ undergo magnetic phase transitions at 2.9 and 3.1 K, respectively. At high temperatures both samples behave as Curie−Weiss paramagnets with a small diamagnetic contribution; the data above 70 K can be described by a modified Curie−Weiss law: $\chi(T) = \chi_{dia} + C/(T - \Theta_{CW})$. The effective magnetic moments m_{eff} determined from least-squares fits to the data are 7.9(1)μ_B (x = 1.0) and 7.8(1)μ_B (x = 1.4); with the Weiss temperatures Θ_{CW} of 1.7(8) K (x = 1.0) and 2.9(5) K (x = 1.4). The effective magnetic moment for both samples is close to the value expected for Eu^{2+} of m_{eff} = 7.94 μ_B, indicating a divalent Eu state in $Eu_xBa_{2-x}Cu_{16}P_{30}$. The inset of Figure 8 shows the isothermal magnetization field dependence at 2 K as magnetic moment per Eu atom. Both Eu-containing samples reach the saturation value expected for Eu^{2+} of m_{sat} = 7.0 μ_B in fields above 3 T. Therefore, all magnetic measurements are consistent with a $4f^7$ (Eu^{2+}) electronic state.

The temperature dependence of the electrical resistivity $\rho(T)$ for $Eu_xBa_{8-x}Cu_{16}P_{30}$ is plotted in Figure 9 normalized to the value at 300 K, $\rho(T)/\rho_{300K}$. The inset shows the low-temperature behavior of the sample $Eu_1Ba_7Cu_{16}P_{30}$ in magnetic fields up to 3 T. The samples with x = 1.0 and x = 1.4 exhibit a similar temperature dependence of the resistivity, although the measured absolute values at 300 K differ by a factor of 2.5, presumably because of a polycrystalline nature of the samples: the specimen with x = 1.0 reaches ρ_{300K} = 2270 $\mu\Omega$ cm, while the sample with x = 1.4 has lower value of ρ_{300K} = 880 $\mu\Omega$ cm. We attribute these variations to uncertainties in form factors, and thus conclude that the intrinsic temperature dependence $\rho(T)$ is similar for both samples. The overall behavior of $\rho(T)$ is metal-like with a positive $d\rho/dT$, except for a weak maximum at around 3 K (cf. inset of Figure 9, not shown for x = 1.4). As mentioned above, the investigated phase $Eu_xBa_{8-x}Cu_{16}P_{30}$ has a deficiency of 2 electrons per formula unit with respect to the charge-balanced Zintl composition. The observed metallic behavior is in agreement with the holes as free charge carriers suggested by electron counting. At temperatures above 50 K charge carriers are mainly scattered by phonons. Thus, the similarity of $\rho(T)$ for different Eu content x at T > 50 K provides evidence for a uniform phonon spectrum for all compositions. This is attributed to the fact that less than 2 of 54 atoms per formula are substituted upon the Ba/Eu exchange. Taking additionally into account that the ratio of the atomic masses of Ba and Eu is close to unity (1:1.107), no drastic changes in the phonon spectrum is expected for the investigated compositions. This assumption was confirmed by specific heat measurements.

The anomalies near 3 K are probably caused by scattering on magnetic fluctuations above the magnetic ordering temperatures. The drop in resistivity below the magnetic ordering temperature is then a consequence of reduced spin-disorder scattering in the ordered state. This assumption is supported by the resistivity measurements on the sample $Eu_1Ba_7Cu_{16}P_{30}$ in magnetic fields (inset of Figure 9). When applying a magnetic field, the resistivity is reduced, which is in agreement with the suppression of spin-disorder scattering because of the field-induced magnetization of the sample.

The specific heat of $Ba_8Cu_{16}P_{30}$, a reference Eu-free compound, is shown in the main part of Figure 10. For the analysis it may be treated as a sum of a phononic and an electronic contribution. The electronic specific heat $c_{el} = 0.076 \cdot T$ J mole^{-1} K^{-1} was estimated from a linear fit to c_p/T vs T^2 for T < 5 K (upper inset of Figure 10). The phononic contribution may be approximated by a sum of one Debye and two Einstein terms. The Debye term approximates the acoustic phonon modes, while the optic modes are described by an Einstein term. The second Einstein term was added to account for the possibility of thermal vibrations of the Eu and Ba cations inside the cages. A least-squares fit to the data yielded a Debye temperature Θ_D = 235 K. The corresponding Einstein temperatures are Θ_{E1} = 449 K and Θ_{E2} = 85 K. The sum of the phononic and electronic contributions is shown as a line in the main plot of Figure 10. The low-temperature Einstein contribution with Θ_{E2} = 85 K suggests the presence of local vibrations of the guest atoms inside the cages, similar to conventional tetrel clathrates.[8d,28] The low-temperature Einstein contribution may also be determined directly from the specific-heat data. A plot of c_p/T^3 vs T reveals a broad peak at around 18 K (lower right inset of Figure 10). In this type of diagram an Einstein contribution shows up as a maximum at 0.20 Θ_E, while a pure Debye term is constant at low T.[29] From the maximum, a value of Θ_{E2} = 89 K is determined, in good agreement with the 85 K obtained from a fit to the data.

The high-temperature specific heat of the Eu-containing samples is very similar to that of $Ba_8Cu_{16}P_{30}$. Above 15 K the data for different x fall on top of each other. It is assumed that rattling of guest atoms in larger 24-vertex cages of type-I clathrates

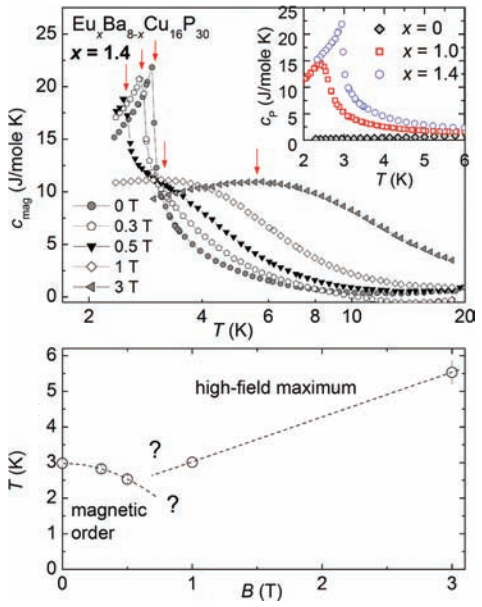

Figure 11. Top: low-temperature specific heat of $Eu_xBa_{8-x}Cu_{16}P_{30}$. The main plot shows the behavior of the sample with $x = 1.4$ in magnetic fields up to 3 T. The arrows mark the magnetic ordering temperature in low fields and the maximum in the Schottky contribution at higher B. The inset displays the low-T data for all samples ($x = 0$, 1, 1.4) in zero field. Bottom: phase diagram showing the evolution of the ordering temperature and the maximum in c_{mag} with increasing field. From our data we cannot deduce the behavior in the regions labeled by questions marks.

constitutes major Einstein contribution to heat capacity, whereas motion of guests in smaller pentagonal dodecahedral cages is negligible.[28b] For $Ba_8Cu_{16}P_{30}$ and $Eu_xBa_{8-x}Cu_{16}P_{30}$ the 24-vertex cages host Ba atoms only; therefore, similar values for the phonon Einstein contribution are expected for all these cages. Mixed occupation of small cages by Ba and Eu atoms should not strongly affect the phonon spectrum because of close atomic masses of Ba and Eu. The electronic contribution at high temperature stems from similar charge carrier concentration and should not vary significantly within the homogeneity range $Eu_xBa_{8-x}Cu_{16}P_{30}$. In turn, the low temperature electronic contribution may be affected by the presence of localized f electrons. In addition, at low temperatures the Eu-containing samples exhibit λ-type anomalies near the magnetic ordering temperatures determined from susceptibility measurements (inset of Figure 11, top). These anomalies confirm the presence of magnetic phase transitions. Subtracting the specific heat of the reference compound ($x = 0$) from the data, the field-dependent magnetic contribution to the specific heat c_{mag} is obtained.

The main plot of Figure 11 (top) shows the magnetic contribution to the specific heat for the sample $Eu_{1.4}Ba_{6.6}Cu_{16}P_{30}$ in applied *dc* magnetic fields up to 3 T. At a field of 0.5 T a shoulder appears just above the phase transition, while the λ-type anomaly still persists. In fields above 1 T the shoulder has turned into a broad hump, which shifts to higher temperature with increasing field. Similar results are obtained for the samples with $x = 1$ (not shown). Application of a small field induces a shift of the anomaly to lower temperatures. The observed behavior is typical for antiferromagnets with a low ordering temperature: upon application of an external magnetic field, initially, the transition temperature is reduced (Figure 11, bottom).[30] At larger fields the system is driven to an induced paramagnetic state. For $B \geq 0.5$ T the Zeeman splitting of the ground-state multiplet shows up as a Schottky contribution to the specific heat.

Assuming a constant c_{mag}/T below the lowest measured temperature of approximately 2 K, the entropy associated with the phase transitions can be estimated. For the sample with $x = 1$ approximately 92% of the value expected for complete ordering of Eu^{2+} is reached at 10 K. Therefore, we conclude that the transition is accompanied by complete ordering of the Eu^{2+} spins.

CONCLUSIONS

Chemical features and physical properties of the tetrel-free clathrate $Eu_xBa_{8-x}Cu_{16}P_{30}$ ($0 \leq x \leq 1.5$) are explored. In the crystal structure, the Eu atoms occupy small pentagonal-dodecahedral cages. Its unique Cu−P framework shows segregation of phosphorus atoms that form finite fragments P_{18} and P_{12} and causes formation of the orthorhombic $\sqrt{2} \times 1 \times 2\sqrt{2}$ clathrate-I superstructure. $Eu_xBa_{8-x}Cu_{16}P_{30}$ demonstrates that clathrate chemistry is not limited to tetrel-based frameworks, and new clathrates may be found utilizing an appropriate combination of other than Group 14 elements. Examples corroborating this assumption can be found among recently reported clathrate-I $Cs_8Zn_{18}Sb_{28}$[31] as well as inverse clathrates-I phases where more than 70% of tetrel framework atoms are substituted with a combination of (Ga,In)-(P,As,Sb).[3e] Near 3 K, $Eu_xBa_{8-x}Cu_{16}P_{30}$ undergoes a magnetic phase transition to an antiferromagnetically ordered state. Owing to the low transition temperatures the samples are driven to an induced paramagnetic state by application of a relatively weak magnetic field, as apparent from a Schottky contribution to the specific heat in fields above 0.5 T. The specific heat of the Eu-free reference compound $Ba_8Cu_{16}P_{30}$ suggests the presence of local vibrations of the guest atoms inside their cages. However, the semiconducting behavior observed earlier[4] could not be reproduced. Instead, metal-like resistivity was found for all samples, as expected from the deficiency of 2 electrons per formula unit for the stoichiometric system. Therefore, in particular large thermopower values and consequently a superior thermoelectric performance are not expected for the investigated phase.

ASSOCIATED CONTENT

Supporting Information. Crystallographic data in CIF format. This material is available free of charge via the Internet at http://pubs.acs.org.

AUTHOR INFORMATION

Corresponding Author

*E-mail: kkovnir@ucdavis.edu. Phone: +1-530-752-5563. Fax: +1-530-752-8995.

Present Addresses

⊥Laboratory of Inorganic Chemistry, ETH Zurich, 8093 Zurich, Switzerland.

ACKNOWLEDGMENT

The authors express their gratitude to Ms. P. Scheppan and Dr. U. Burkhardt for the metallographic and EDX analyses; Ms. S. Müller and Dr. R. Niewa for DSC investigation. The Competence Group Structure of the MPI CPfS is acknowledged for the help with powder X-ray diffraction data collection. K. K.

acknowledges the Max-Planck-Gesellschaft for a research fellowship. A. V. S. acknowledges the support of the Russian Foundation of Basic research and S. P. acknowledges the Austrian Science Foundation (project P19458_N16).

REFERENCES

(1) (a) Jeffrey, G. A. In *Inclusion Compounds*; Atwood, J. L., Davies, J. E. D., MacNicol, D. D., Eds.; Academic Press Inc.: London, U.K., 1984. (b) Müller, A.; Reuter, H.; Dillinger, S. *Angew. Chem., Int. Ed. Engl.* **1995**, *34*, 2328–2361.

(2) Kasper, J. S.; Hagenmuller, P.; Pouchard, M.; Cros, C. *Science* **1965**, *150*, 1713–1714.

(3) (a) Bobev, S.; Sevov, S. C. *J. Solid State Chem.* **2000**, *153*, 92–105. (b) Kovnir, K. A.; Shevelkov, A. V. *Usp. Khimii.* **2004**, *73*, 999–1015. (c) Kovnir, K. A.; Shevelkov, A. V. *Russ. Chem. Rev.* **2004**, *73*, 923–938. (d) Beekman, M.; Nolas, G. S. *J. Mater. Chem.* **2008**, *18*, 842–851. (e) Shevelkov, A. V.; Kovnir, K. *Struct. Bonding (Springer: Berlin)* **2011**, *139*, 97–142.

(4) Dünner, J.; Mewis, A. *Z. Anorg. Allg. Chem.* **1991**, *621*, 191–196.

(5) Huo, D.; Sasakawa, T.; Muro, Y.; Takabatake, T. *Appl. Phys. Lett.* **2003**, *82*, 2640–2642.

(6) (a) Slack, G. A. In *CRC Handbook of Thermoelectrics*; Rowe, D. M., Ed.; CRC Press: Boca Raton, FL, 1995. (b) Nolas, G. S.; Slack, G. A.; Schjuman, S. B. In *Recent Trends in Thermoelectric Materials Research*; Tritt, T.M., Ed.; Academic Press: San Diego, CA, 2001; (c) Shevelkov, A. V. *Russ. Chem. Rev.* **2008**, *77*, 1–19. (d) Beekman, M.; Nolas, G. S. *J. Mater. Chem.* **2008**, *18*, 842–851. (e) Christensen, M.; Johnsen, S.; Iversen, B. B. *Dalton Trans.* **2010**, *39*, 978–992.(f) Paschen, S.; Godart, C.; Yu. Grin In *Complex Metallic Alloys. Fundamentals and Applications*; Dubois, J.-M., Belin-Ferré, E., Eds.; Wiley-VCH: Weinheim, Germany, 2011.

(7) (a) Pacheco, V.; Carrillo-Cabrera, W.; Tran, V. H.; Paschen, S.; Grin, Yu. *Phys. Rev. Lett.* **2001**, *87*, 099601. (b) Paschen, S.; Gspan, C.; Grogger, W.; Dienstleder, M.; Laumann, S.; Pongratz, P.; Sassik, H.; Wernisch, J.; Prokofiev, A. *J. Cryst. Growth* **2008**, *310*, 1853–1858. (c) Paschen, S.; Budnyk, S.; Köhler, U.; Prots, Yu.; Hiebl, K.; Steglich, F.; Grin, Yu. *Phys. B* **2006**, *383*, 89–92.

(8) (a) Paschen, S.; Carrillo-Cabrera, W.; Bentien, A.; Tran, V. H.; Baenitz, M.; Grin, Yu.; Steglich, F. *Phys. Rev. B* **2001**, *64*, 214404. (b) Pacheco, V.; Bentien, A.; Carrillo-Cabrera, W.; Paschen, S.; Steglich, F.; Grin, Yu. *Phys. Rev. B* **2005**, *71*, 165205. (c) Bentien, A.; Pacheco, V.; Paschen, S.; Grin, Yu.; Steglich, F. *Phys. Rev. B* **2005**, *71*, 165206. (d) Sales, B. C.; Chakoumakos, B. C.; Jin, R.; Thompson, J. R.; Mandrus, D. *Phys. Rev. B* **2001**, *63*, 245113.

(9) (a) Mudryk, Ya.; Rogl, P.; Paul, C.; Berger, S.; Bauer, E.; Hilscher, G.; Godart, C.; Noel, H.; Saccone, A.; Ferro, R. *Phys. B* **2003**, *328*, 44–48. (b) Cohn, J. L.; Nolas, G. S.; Fessaditis, V.; Metcalf, T. H.; Slack, G. A. *Phys. Rev. Lett.* **1999**, *82*, 779–782. (c) Zhang, Y.; Lee, P. L.; Nolas, G. S.; Wilkinson, A. P. *Appl. Phys. Lett.* **2002**, *80*, 2931–2933. (d) Mudryk, Ya.; Rogl, P.; Paul, C.; Berger, S.; Bauer, E.; Hilscher, G.; Godart, C.; Noel, H. *J. Phys.: Condens. Matter* **2002**, *14*, 7991–8004. (e) Demchyna, R.; Köhler, U.; Prots, Yu.; Schnelle, W.; Baenitz, M.; Burkhardt, U.; Paschen, S.; Schwarz, U. *Z. Anorg. Allg. Chem.* **2006**, *632*, 73–78. (f) Köhler, U.; Demchyna, R.; Paschen, S.; Schwarz, U.; Steglich, F. *Phys. B* **2006**, *378*−*380*, 263–264. (g) Condron, C. L.; Porter, R.; Guo, T.; Kauzlarich, S. M. *Inorg. Chem.* **2005**, *44*, 9185–9191. (h) Condron, C. L.; Kauzlarich, S. M.; Gascoin, F.; Snyder, G. J. *Chem. Mater.* **2006**, *18*, 4939–4945. (i) Woods, G. T.; Martin, J.; Beekman, M.; Hermann, R. P.; Grandjean, F.; Keppens, V.; Leupold, O.; Long, G. J.; Nolas, G. S. *Phys. Rev. B* **2006**, *73*, 174403. (j) Phan, M. H.; Franco, V.; Chaturvedi, A.; Stefanoski, S.; Kirby, H.; Nolas, G. S.; Srikanth, H. *J. Appl. Phys.* **2010**, *107*, 09A910.

(10) Akselrud, L. G.; Zavalii, P. Yu.; Grin, Yu.; Pecharsky, V. K.; Baumgartner, B.; Wölfel, E. *Mater. Sci. Forum* **1993**, *133*−*136*, 335.

(11) Gelato, L. M.; Parthé, E. *J. Appl. Crystallogr.* **1987**, *20*, 139.

(12) Dünner, J.; Mewis, A. *J. Less-Common Met.* **1990**, *167*, 127–134.

(13) Mewis, A. *Z. Naturforsch. B* **1980**, *35*, 141–145.

(14) Emsley, J. *The Elements*, 3rd ed.; Clarendon Press: Oxford, U.K., 1998.

(15) Liebau, F. *Structural Chemistry of Silicates* − *Structure, Bonding, and Classification*; Springer: Berlin, Germany, 1985.

(16) (a) Shatruk, M. M.; Kovnir, K. A.; Lindsjö, M.; Presniakov, I. A.; Kloo, L. A.; Shevelkov, A. V. *J. Solid State Chem.* **2001**, *161*, 233–242. (b) Carrillo-Cabrera, W.; Budnyk, S.; Prots, Yu.; Grin, Yu. *Z. Anorg. Allg. Chem.* **2004**, *630*, 2267–2276. (c) Dubois, F.; Fässler, T. F. *J. Am. Chem. Soc.* **2005**, *127*, 3264–3265. (d) Zaikina, J. V.; Kovnir, K. A.; Sobolev, A. V.; Presniakov, I. A.; Prots, Yu.; Baitinger, M.; Schnelle, W.; Olenev, A. V.; Lebedev, O. I.; Van Tendeloo, G.; Grin, Yu.; Shevelkov, A. V. *Chem.—Eur. J.* **2007**, *13*, 5090–5099.

(17) *International Tables for Crystallography*; Hahn, T., Ed.; Kluwer: Dordrecht, The Netherlands, 1989; Vol. A.

(18) Bärnighausen, H. *MATCH* **1980**, *9*, 139–175.

(19) (a) Shatruk, M. M.; Kovnir, K. A.; Shevelkov, A. V.; Popovkin, B. A. *Russ. J. Inorg. Chem.* **2000**, *45*, 203–209. (b) Kovnir, K. A.; Sobolev, A. V.; Presniakov, I. A.; Lebedev, O. I.; Van Tendeloo, G.; Schnelle, W.; Grin, Yu.; Shevelkov, A. V. *Inorg. Chem.* **2005**, *44*, 8786–8793.

(20) Inorganic Crystal Structure Database (ICSD) Version 2010−2.

(21) (a) von Schnering, H. G.; Menke, H. *Angew. Chem., Int. Ed. Engl.* **1972**, *11*, 43–44. (b) Menke, H.; von Schnering, H. G. *Z. Anorg. Allg. Chem.* **1973**, *395*, 223–238. (c) Menke, H.; von Schnering., H. G. *Z. Anorg. Allg. Chem.* **1976**, *424*, 108–114.

(22) von Schnering, H. G.; Hönle, W. *Chem. Rev.* **1988**, *88*, 243–273.

(23) Chen, X.; Zhu, L.-P.; Yamanaka, S. *J. Solid State Chem.* **2003**, *173*, 449–455.

(24) (a) Zaikina, J. V.; Kovnir, K. A.; Schwarz, U.; Borrmann, H.; Shevelkov, A. V. *Z. Kristallogr. NCS* **2007**, *222*, 177–179. (b) Zaikina, J. V.; Kovnir, K. A.; Burkhardt, U.; Schnelle, W.; Haarmann, F.; Schwarz, U.; Grin, Yu.; Shevelkov, A. V. *Inorg. Chem.* **2009**, *48*, 3720–3730.

(25) *Chemistry, Structure and Bonding of Zintl Phases and Ions*; Kauzlarich, S.M., Ed.; VCH: New York, 1996.

(26) Kovnir, K.; Reiff, W. M.; Menushenkov, A. P.; Yaroslavtsev, A. A.; Chernikov, R. V.; Shatruk, M. *Chem. Mater.* **2011**, *23*, 3021–3024.

(27) Actual Eu content $x = 1.4$ was established by a combination of magnetic and heat capacity measurements. Sample $Eu_1Ba_7Cu_{16}P_{30}$ was used as a reference.

(28) (a) Avila, M. A.; Suekuni, K.; Umeo, K.; Fukuoka, H.; Yamanaka, S.; Takabatake, T. *Phys. Rev. B* **2006**, *74*, 125109. (b) Aydemir, U.; Candolfi, C.; Borrmann, H.; Baitinger, M.; Ormeci, A.; Carrillo-Cabrera, W.; Chubilleau, C.; Lenoir, B.; Dauscher, A.; Oeschler, N.; Steglich, F.; Grin, Yu. *Dalton Trans.* **2010**, *39*, 1078–1088. (c) Falmbigl, M.; Rogl, G.; Rogl, P.; Kriegisch, M.; Müller, H.; Bauer, E.; Reinecker, M.; Schranz, W. *J. Appl. Phys.* **2010**, *108*, 043529.

(29) Ashcroft, N.W.; Mermin, N.D. *Solid State Physics*; Saunders: Philadelphia, PA, 1976.

(30) Yosida, K. *Theory of Magnetism*; Springer: Berlin, Germany, 1996.

(31) Liu, Y.; Wu, L.-M.; Li, L.-H.; Du, S.-W.; Corbett, J. D.; Chen, L. *Angew. Chem., Int. Ed.* **2009**, *48*, 5305–5308.